Available online at www.sciencedirect.com
SCIENCE DIRECT®
International Journal of Heat and Mass Transfer 49 (2006) 1946–1957
International Journal of HEAT and MASS TRANSFER
www.elsevier.com/locate/ijhmt

Free convection frost growth in a narrow vertical channel

G. Tanda *, M. Fossa

Dipartimento di Ingegneria della Produzione, Termoenergetica e Modelli Matematici (DIPTEM), Università degli Studi di Genova, via all'Opera Pia 15a, I-16145 Genova, Italy

Received 8 November 2004
Available online 10 January 2006

Abstract

Processes involving heat transfer from a humid air stream to a cold plate, with simultaneous deposition of frost, are of great importance in a variety of refrigeration equipment. In this work, frost growth on a vertical plate in free convection has been experimentally investigated. The cold plate (0.095 m high, 0.282 m wide) was placed in a narrow (2.395 m high, 0.01 m deep) vertical channel open at the top and bottom in order to permit the natural circulation of ambient air. The cold plate temperature and the air relative humidity were varied in the −40 to −4 °C and 31–85% range, respectively, with the air temperature held fixed at 27 °C (±1 °C). The main quantities (thickness, temperature and mass of frost, heat flux at the cold plate), measured during the time evolution of the process, are presented as functions of the input parameters (relative humidity and cold plate temperature); in particular, the role exerted by the plate confinement on the frost growth is discussed. Data are recast in order to identify compact parameters able to correlate with good accuracy frost thickness, mass and density data.

Keywords: Frost; Vertical channel; Free convection; Heat/mass transfer

1. Introduction

Frost formation occurs when humid air passes over a surface whose temperature is below the water freezing temperature. In many engineering applications, frost is undesirable. For example, a frost layer over a heat transfer surface contributes to increase the thermal resistance and reduces the rate of heat transfer. In channel flows, frost may also reduce the flow cross-section and result in a lower mass flow rate of air or even in a flow blockage.

The growth of frost is a complicated transient process in which both heat and mass transfer occur simultaneously. Hayashi et al. [1] identified three different periods in frost formation process: (a) *a crystal growth period*, characterised by a one-dimensional growth of frost crystals in the direction perpendicular to the frosting surface, (b) *a frost layer growth period*, when the frost crystals interact with other crystals resulting in a uniform frost layer, (c) *a frost layer full growth period*, when the frost surface reaches 0 °C and a cyclical process of melting, freezing and deposition occurs until frost formation stops. The time for each period and the shape of frost crystals were found to strongly depend on the cooling surface temperature and the vapour concentration difference between the mean stream and the cooling surface.

The dependence of frost formation on the environmental variables and surface conditions has been studied extensively. Key parameters are the cooling surface temperature and air humidity; typically, changing the cold plate temperature mainly affects the frost thickness, while changing the relative humidity affects both frost thickness and mass rate. As for the role played by other parameters, data provided by previous studies are often not in agreement. Increasing air velocity turned out not to affect frost growth [2], to increase it up to a critical Reynolds number [3], to increase the frost mass rate and not the thickness [4], or to increase both the mass and (slightly) the thickness of frost [5].

* Corresponding author. Tel.: +39 010 3532881; fax: +39 010 311870.
E-mail address: tanda@ditec.unige.it (G. Tanda).

0017-9310/$ - see front matter © 2005 Elsevier Ltd. All rights reserved.
doi:10.1016/j.ijheatmasstransfer.2005.11.010

Nomenclature

DP	densification parameter (Eq. (7)), $\text{min}^{0.5}(\text{kg}_v/\text{kg})^{0.29}$
FGP	frost growth parameter (Eq. (1)), min K
FTP	frost thickness parameter (Eq. (9)), $\text{min}^{0.5}(\text{kg}_v/\text{kg})^{0.71}$
MDP	mass deposition parameter (Eq. (3)), min kg_v/kg
m''	deposited mass (per unit area) of frost, kg/m^2
Rh	relative humidity, %
T	temperature, °C
τ	time, min
ω	humidity ratio, kg_v/kg

Greek symbols

δ	frost thickness, mm
ρ	frost density, kg/m^3

Subscripts

amb	ambient
fs	frost surface
out	outlet air
w	wall (cold surface)

Similar inconsistencies were found for air temperature effects: higher air temperature (holding the humidity ratio constant) yielded lower frost height with [5] and without [6] an increase in mass amount, while in [3] no effect of air temperature on frost growth (for the 5–12 °C range) was found. Moreover, cooling surface conditions (roughness, affinity with water) may affect the formation of frost nuclei [7,8].

Several models for frost growth have been proposed in the literature [9–15]; however, owing to the complexity of the phenomenon, the development of precise predictions of frost growth characteristics as well as of correlations to evaluate frost properties is still a demanding task. Despite the increasing degree of sophistication in the development of new models (accounting for spatial and temporal variations in density and temperature of frost and for supersaturation of vapour at the frost surface) more experimental data seem to be required to check both the assumptions made in the theoretical analyses and the predicted results.

As clearly outlined in some review papers [16,17], frost formation during the forced convection of humid air has been extensively studied, while, on the other hand, only a limited number of investigations deal with mass-heat transfer during natural convection on a surface at subfreezing temperatures. This problem was tackled by Kennedy and Goodman ([18], study of frost formation on a vertical surface), Tajima et al. ([19], flat surface with different orientations), Cremers and Mehra ([20], outer side of vertical cylinders), Tokura et al. ([7], vertical surface). To the authors' knowledge, no data are available for natural convection in channels, despite the practical significance of this phenomenon in such devices as evaporative heat exchangers for cryogenic liquid gasification.

The aim of this paper is to provide better understanding of free convection frost growth inside narrow channels. Experiments were designed to measure the frost thickness, surface temperature, deposited mass and the air-to-frost heat flux at regular time intervals, for a variety of ambient relative humidity and wall temperature conditions, while the ambient temperature was held fixed. The information obtained from the experiments was used to identify conditions for which the heat/mass transfers in the channel are markedly reduced or even suppressed as well as correlations to predict the frost growth, deposited mass and density.

2. The experimental setup

A schematic view of the experimental apparatus is shown in Fig. 1. The entire apparatus and the instrumentation were placed in a large laboratory where relative humidity could be regulated over the 30–90% range at 27 ± 1 °C. The channel, made of Plexiglas and rectangular in shape, had a section of 0.01 m (depth) × 0.36 m (width) and was 2.395 m high: it was open at the top and bottom in order to permit natural circulation of ambient air. The test section, located at 1.3 m from the channel top section and at 1.0 m from the bottom section, consisted of a 0.095 m high, 0.282 m wide, cold plate and three Plexiglas

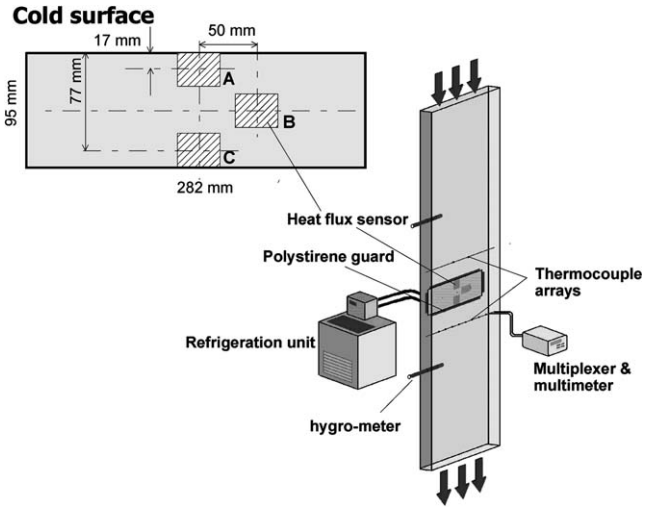

Fig. 1. Schematic layout of the vertical channel and cold plate.

walls forming a channel as deep and as wide as the entrance and exit channels. The aspect ratio of the vertical channel (ratio between the depth and the height) was 0.004175; the aspect ratio of the cooled section of the channel (ratio between the depth of the channel and the height of the cold plate) was 0.1053.

The cold plate was made of copper and cooled by the internal circulation of ethyl alcohol coming from a thermostatic bath. The plate was framed inside a Plexiglas wall and separated from it by 10 mm-thick polystyrene strips to minimise the thermal conduction at the plate boundaries and thus prevent dew and frost formation on surfaces other than the test surface.

Each experiment was conducted with constant values of ambient air temperature and relative humidity and for a given value of the cold plate surface temperature. Namely, the temperature of the ambient air was set at a value in the range 26–28 °C, with variations in time, for each individual test, confined within 0.9 K, while the relative humidity Rh was taken at a value between 31 and 85%, with variations in time, for each individual test, confined within 2% (in Rh units). The surface temperature T_w of the cold plate was varied in the −40 to −4 °C range, with variations in time and along the surface within ±1 °C (at the lowest T_w) and ±0.4 °C (at the highest T_w).

Before test plate cooling, the surface was covered with a thin polyethylene film so that water vapour could not condense on the test plate before the starting of the test. After the prescribed temperature of the plate was reached, the test was started by taking off the film. The standard duration of each test was 7.5 h; the monitored quantities (air, plate and frost temperatures, frost thickness, and heat flux) were measured at regular time intervals (typically 30–45 min for frost thickness and air and plate temperatures, and 5–15 min for frost surface temperature and heat flux) after the test inception.

The relative humidity of the convective air flow was measured by capacitance hygrometers, carefully calibrated in the 10–95% range and positioned at the inlet and outlet of the test section. The estimated uncertainty (at the 95% confidence level, 20/1 odds) in air relative humidity was 2% (in Rh units). The surface temperature of the cold plate was measured by five thermocouples, fitted inside small holes drilled into the wall material positioned as close as possible to the exposed surface. Numerous fine-gauge thermocouples were employed to evaluate the temperature of the air flow at the test section inlet and outlet. Additional thermocouples were located in the Plexiglas wall opposite to the cold plate (to allow the evaluation of the thermal radiation exchange) and in the material surrounding the cold plate (to allow the checking of thermal conduction to the plate from the surrounding). Two infrared thermometers were used to measure the frost layer surface temperature at the plate midheight: the mean frost surface temperature was calculated as the average of the two individual measurements. The estimated uncertainty (at 20/1 odds) in temperature measurements was 0.1 °C for thermocouples and 0.8 °C for infrared thermometers; these sensors were characterised by the largest uncertainties in the early stage of frost formation (especially at low humidity) owing to the strong variations of the emittance of the thin frost layer. This last quantity, for a compact frost layer, was measured to be 0.95 by a separate set of experiments.

The thickness of the frost layer was continuously monitored at the three locations A, B, and C (see Fig. 1) corresponding to the positions of the heat flux sensors. Two alternative types of sensors were used: contact sensors and optical sensors. The contact probe consisted of a 1 mm-dia needle connected to a micrometer and moved from the Plexiglas wall (facing the cold plate) towards the frost surface until the contact was visually observed. A nylon tip needle was employed to prevent frost melting. The optical probe consisted of a co-axial glass fibre, whose tip, fitted by a lens, emits a pulsed red light. The intensity of back reflected light, proportional to the distance from the target and to the reflectivity of the target, exhibits a peak value when the distance from the target is equal to the lens focal length. In order to maximise the sensitivity of the device, the probe was mounted on a micrometer; a set of measurements (6 at least) was performed at various distances from the target so as to infer, by regression analysis of individual signal values, the position of the sensor corresponding to the maximum light intensity. The measurement technique based on the contact probes is more time consuming (great care is required to identify the contact point without damaging the growing frost layer) but relatively accurate (20/1 odds uncertainty about 0.35 mm) for every surface condition of frost; on the other hand, the use of the optical probe gives rise to greater uncertainty (between 1 and 2 mm) when the frost surface is rough and porous (owing to the variation of reflectance properties of the growing frost layer), whereas for compact, flat and uniform frost layers uncertainty drops to only 0.15 mm. As further validation of the described thickness measurements, additional measurements were made, by using two shielded, 0.5 mm-dia thermocouples connected to micrometers so as to travel through the cold plate (inside small holes) into the frost layer up to the frost/air interface: owing to the destructive nature of this procedure, it was applied only at the end of each test. Once established the good agreement among the different measurement procedures under standard operating conditions (presence of compact and uniform frost layer at various thicknesses), the majority of the presented thickness measurements were performed by using the contact probes, since their accuracy was found to depend only slightly on the input parameters (air temperature/humidity and cold plate temperature).

The heat flux entering the cold plate was measured by three heat flux sensors (size 1 cm^2, thickness 0.15 mm) flush-mounted on the test surface at different positions (A, B, and C) as shown in Fig. 1. Since the thermal resistance of each heat flux sensor (about 0.002 K m^2/W) is very low as compared to the air side (or frost side) thermal resistance, their presence was expected not to locally alter

the frost formation phenomenon. For the same reason, the thin lead wires were accommodated into little holes drilled across the cold plate and were not exposed to the humid air flow. The uncertainty (at 20/1 odds) in heat flux, estimated according to conductive and convective mode calibrations, was, in percentage, equal to 10%.

The deposited mass of frost was measured by a precision balance (having a resolution of 10^{-5} kg) after the frost had been scraped off the plate at the end of each test. In order to recover the temporal variation of the frost mass, additional runs were performed at different time durations and the mass was weighed at the end of each of them.

3. Results and discussion

A former set of experiments [21–23] conducted by the same authors for a larger channel (depth double of that considered here) and same cooling surface, same test duration, same relative humidity range and cold plate temperature between −13 and −4 °C, led to the following considerations:

- the thickness of the growing frost layer was only slightly affected by location and was found to increase with the square root of time. Largest thickness values occurred at the highest relative humidities and air-to-plate temperature differences; however, relative humidity, when higher then 50%, exerted only a limited effect on frost thickness;
- the surface temperature of the growing frost layer attained very quickly an asymptotic value close to the freezing temperature at relatively high relative humidity. Conversely, at the lowest relative humidities, frost surface temperature was found to increase very slowly with time;
- deposited mass of frost increased linearly with time and was markedly affected by the relative humidity and only slightly affected by the air-to-plate temperature difference;
- the heat flux from air to the cold plate during frost formation was markedly reduced, at the highest relative humidities, during the first two hours from test inception; then a common value was reached. Only slight heat flux reductions (or even enhancements) were observed at the lowest relative humidities. At the same relative humidity, lowest cold plate temperatures yielded largest heat flux decreases with time.

Results for frost formation inside the channel with a depth of 0.02 m [21–23] were qualitatively similar to those obtained by other authors (see for instance [7,20]) for the free convection frost formation on vertical surfaces without confinement. It is argued that the cold plate confinement in a channel of such width induced only minor modification to the frost growth process. Indeed, the growing frost layer, over the investigated time interval (7.5 h), did not significantly obstruct the flow passage, without reductions in the humid air, convected into the channel, feeding the mass transfer process. As the channel depth was reduced from 0.02 to 0.01 m, significant alterations in frost growth were observed, with features strictly related to the values of driving parameters (air relative humidity, cold plate temperature).

3.1. Frost layer outline

Fig. 2 schematically reports typical outlines of the frost layer. Fig. 2a shows a nearly uniform frost growth that progressively develops in the direction normal to the cold plate; this situation, typically observed for free convection in unconfined, vertical plane [7] and cylindrical [20] surfaces and in relatively wide channels [21–23], was typically encountered, for the present geometry, at the highest cold plate temperatures. This regular and uniform frost growth is not able to alter the convection inside the channel at the lowest humidities (owing to the thin layer of deposited frost) while it can yield reductions in the buoyant flow at the highest humidities (owing to the reduced flow passage area and air-to-frost temperature difference). Conversely, low cold plate temperatures combined with relatively high humidities promote a frost growth that is fairly uniform only during the very early stage of the transient; once the deposited frost has occupied a significant part of the free-flow area (say 50% of the available flow passage), the mass transfer still occurs at the leading edge of the cold plate (upper positions) while it ceases downstream owing to the strong reduction in the convective air flow rate, with the corresponding frost outline depicted in Fig. 2b.

Fig. 3 shows the typical frost growth occurring under the different circumstances described in Fig. 2. A mono-

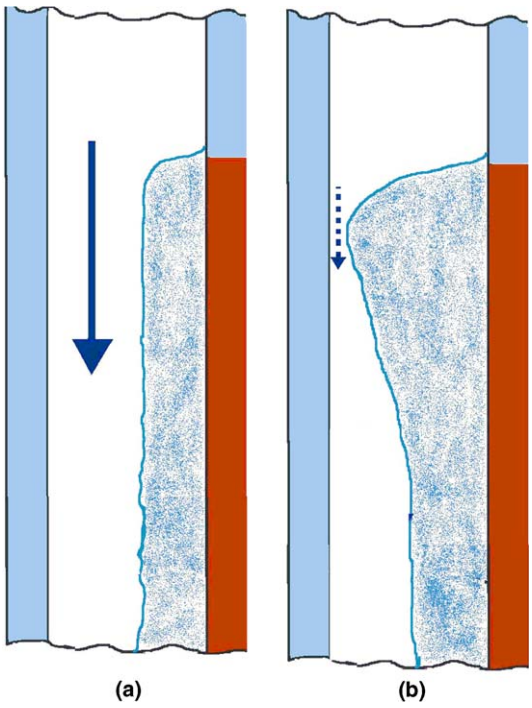

Fig. 2. Typical outlines of the frost layer. (a) Uniform frost growth and (b) frost growth with flow obstruction at the leading edge.

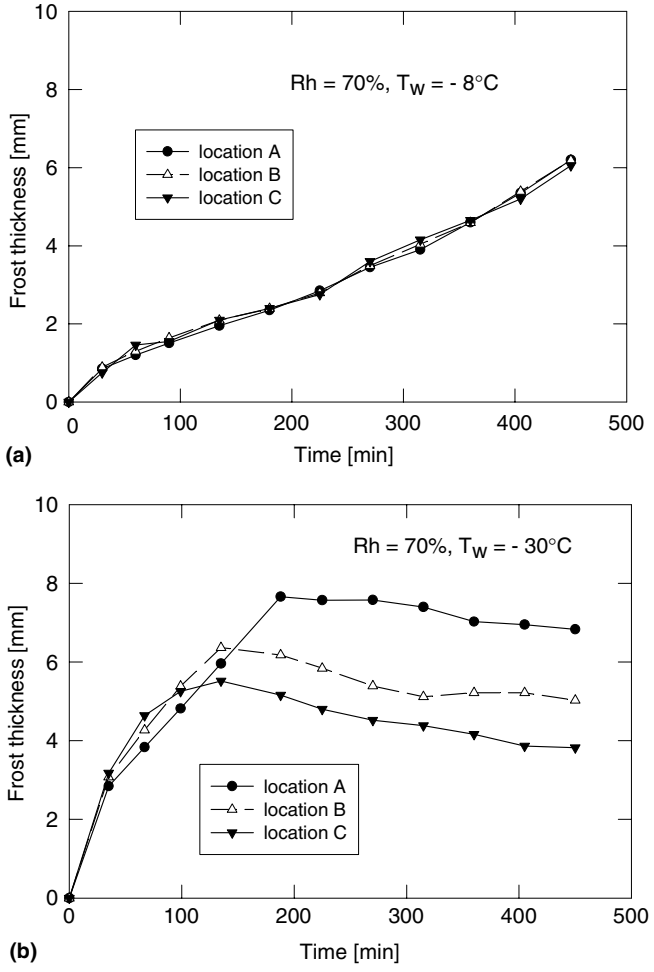

Fig. 3. Frost thickness versus time at different elevations (A, B, and C) and air relative humidity Rh = 70%; (a) cold plate temperature $T_w = -8$ °C and (b) cold plate temperature $T_w = -30$ °C.

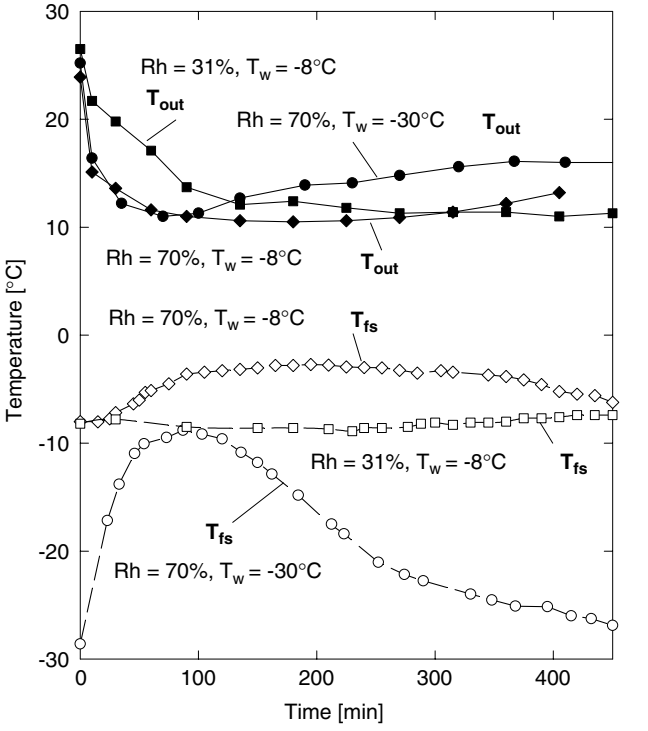

Fig. 4. Mean air temperature downstream of the cold plate (T_{out}, closed symbols) and frost surface temperature (T_{fs}, open symbols) at different Rh and T_w.

tonic increase in frost thickness, practically independent of plate location, is observed for Rh = 70% and $T_w = -8$ °C (Fig. 3a). As the cold plate temperature is decreased ($T_w = -30$ °C, Fig. 3b), the frost thickness grows faster up to the contact with the opposite plate, at an elevation upstream of the probe locations. From this point on, the frost thickness stops to increase (first at the lowest probe location and then at the highest one) and even decreases, probably owing to densification processes.

Similar considerations are reflected in the graph of Fig. 4, where the outlet air temperature T_{out} (evaluated as the average of nine independent measurements over the outside section) and the frost surface temperature T_{fs} are plotted versus time, again for Rh = 70% ($T_w = -8$ °C and −30 °C) and for Rh = 31% ($T_w = -8$ °C). At a relatively high cold plate temperature (−8 °C) and low humidity (31%), the thin frost layer maintains the temperature of the cold plate, while the outlet temperature of the buoyant air flow decreases to a quasi-steady value (about 11 °C). When the humidity is high (70%), the frost surface temperature first increases from the initial value (−8 °C) towards the freezing temperature and then inverts the trend, as the frost thickness increases and the free flow area and the heat/mass convection coefficients are progressively reduced. The air temperature downstream the cold plate quickly decreases to about 10 °C and then increases slightly as a result of a decreased rate of convection heat transfer. At the lower cold plate temperature (−30 °C) and high humidity (70%), convection is suppressed within a short transient. As a consequence, the outlet air temperature, after a rapid decrease (to about 10 °C), shows a marked increase with time while the temperature of frost surface, after the attainment of a maximum value (about −9 °C), rapidly tends to the cold plate temperature.

3.2. Mean frost thickness

The mean frost thickness (evaluated as the average of the three local measurements) versus time is reported, for different values of the cold plate temperature T_w, in Fig. 5. Three values of the air relative humidity are considered, namely Rh = 31% (Fig. 5a), 52% (Fig. 5b) and 70% (Fig. 5c). Generally speaking, during the early transient (and throughout the whole transient at low humidities) frost thickness grows approximately with the square root of time; lower cold plate temperatures typically lead to higher frost thicknesses, while relative humidity, when exceeding about 50%, affects frost thickness only slightly. The ascending–descending profiles pertain to conditions for which the growing frost obstructs the flow passage close to the cold plate leading edge (as shown in Fig. 2b): the

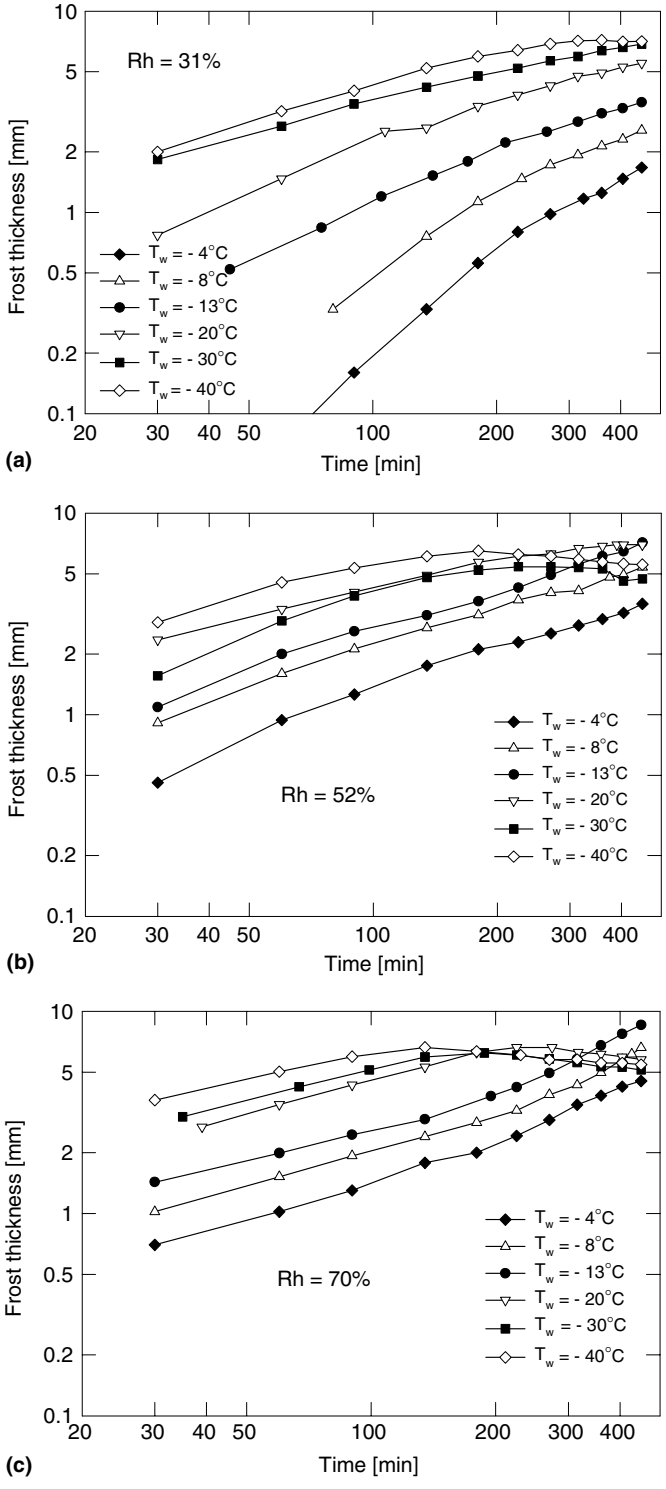

Fig. 5. Mean frost thickness vs. time at different T_w. (a) Rh = 31%, (b) 52%, and (c) 70%.

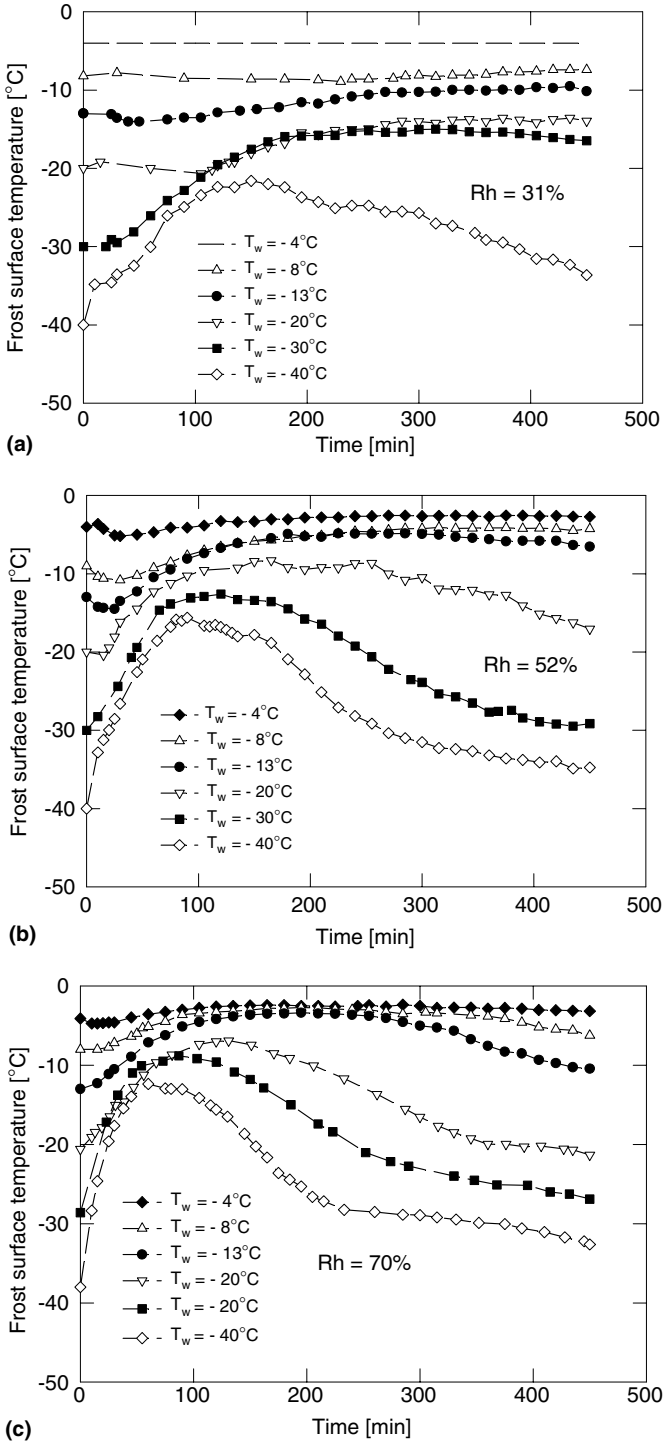

Fig. 6. Frost surface temperature T_{fs} vs. time at different T_w. (a) Rh = 31%, (b) 52%, and (c) 70%.

relative maximum of the mean thickness was about 7 mm, with the channel depth completely filled by frost close to the leading edge and filled at 50% close to the trailing edge. It is worth noting that a regular frost growth (as depicted in Fig. 2a) is characterised by a monotonic increase in the mean thickness with time: the maximum value of the mean thickness was achieved for Rh = 70%, $T_w = -13$ °C, and turned out to be, at the end of the test, 8.2 mm, uniformly distributed (±1 mm) over the cold plate.

3.3. Frost surface temperature

Fig. 6 shows the temperature T_{fs} of the frost surface (measured at the cold plate midheight) versus time, for dif-

ferent values of the cold plate temperature T_w and three different humidity Rh levels. Measurements during the first 30 min of the frost growth (and during the whole test at Rh = 31% and $T_w = -4$ °C) were made critical by the residual reflectance of the copper cold plate affecting the signal provided by the infrared thermometer. The typical trend of T_{fs} during the frost growth on a cold surface exposed to a free convective air flow consists in a gradual increase from the initial value (T_w) towards the freezing temperature (0 °C), as observed at the lowest humidity (Fig. 6a), or intermediate humidities (Fig. 6b) and high cold plate temperatures. When the convective air flow is reduced or even suppressed, the temperature of the frost surface, not efficiently heated by the buoyant air flow, stops to increase and turns towards the value of the opposite frost interface (T_w) owing to the thermal conduction through the frost layer: this is particularly evident at the lowest cold plate temperatures and almost over the whole range of T_w at the highest humidity (Fig. 6c). The frost surface temperature reversal forebodes the flow blockage in the channel, that usually takes place from one to two hours later.

The map plotted in Fig. 7 reports the conditions (cold plate temperature and air relative humidity) for which the inversion of the profile of frost surface temperature occurs within a given time from the test inception. The zone **I** identifies conditions for which T_{fs} starts to decrease during the first 90 min: from this point on, the buoyant air flow is virtually suppressed and mass and heat transfer to the frost surface tend to low values; the frost outline is qualitatively represented by Fig. 2b. Increasing the Roman number (from **II** to **IV**) corresponds to conditions for which the inversion of T_{fs} profile happens later (from 90 to 150 min, zone **II** or from 150 to 300 min, zone **III**) or does not occur (zone **IV**). When the frost surface temperature increases monotonically or starts to decrease after a sufficiently long time from test inception (say 150 min) the frost grows uniformly over the plate, as outlined in Fig. 2a.

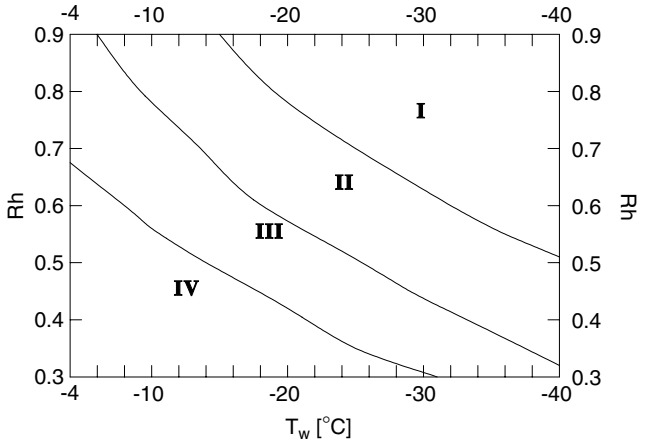

Fig. 7. Rh–T_w plane identifying conditions for which T_{fs} shows a relative maximum vs. time. **I**: T_{fs} maximum within 90 min from frost growth inception, **II**: within 90–150 min, **III**: within 150–300 min, **IV**: no T_{fs} maximum.

Hence, when the input state in the Rh–T_w falls in zone **III** or **IV**, a uniform frost growth is foreseen; conversely, input conditions corresponding to zone **I** or **II** will probably result in irregular frost growth, featured by the blockage of the air flow due to the frost accumulated close to the leading edge of the cold plate.

3.4. Heat flux at the cold plate/frost interface

Attention is now turned to heat flux measured at the plate/frost interface. This quantity has a great importance since frost accumulation acts as a thermal resistance affecting the heat transfer exchange between the plate and the air. As described in Section 2, three plane heat flux sensors were attached to the cold plate at different elevations. Generally speaking, the sensors at locations B (midheight) and C (close to the trailing edge) gave results close to each other, while the sensor located close to the leading edge (A) recorded values with a similar trend but at higher levels, owing to the higher heat/mass transfer coefficient in that region.

Fig. 8 shows heat flux measurements performed at the midheight of the plate (location B, at the same elevation as the frost surface temperature measurement). Each plot refers to heat flux variations in time at a given cold plate temperature and various Rh values. Each profile reflects the interaction between complex (and often conflicting) phenomena which act during frost formation: the spot sublimation of first crystals yielding sudden increases of heat transfer rate in the first few seconds of test (not reported in the graphs owing to the strong fluctuations in time of the signal), the thickening of the frost layer (that increases the thermal resistance of the layer and that can reduce the free flow passage), and the densification of the layer (that increases the mean density and thermal conductivity, so reducing the thermal resistance).

Fig. 8a shows the heat flux at the highest cold plate temperature ($T_w = -4$ °C). Heat flux fluctuations in time are probably due to local frost densification. Increasing the humidity leads to a denser frost layer and a higher heat transfer rate, despite the larger thickness. Significant heat flux reduction is observed only for Rh higher than 70% and during the last part of the transient, when the growing frost layer induces a reduction of the buoyant, down-moving, air flow.

For $T_w = -13$ °C (Fig. 8b), heat flux profiles, after a short transient, attain a common behaviour at any Rh value; then, after a time period of about 180–200 min from frost growth inception, larger humidities lead to thicker frost layers which contribute, when the frost occupies a significant part of the channel, to reduce the air flow and, consequently, the heat flux. The value (103 W/m^2) recorded at the end of the test at $T_w = -13$ °C was the minimum among the performed experiments and corresponds to the maximum frost thickness (from 7.7 to 9 mm, mean 8.2 mm) registered in the course of the experiments. As the cold plate temperature is further decreased ($T_w =$

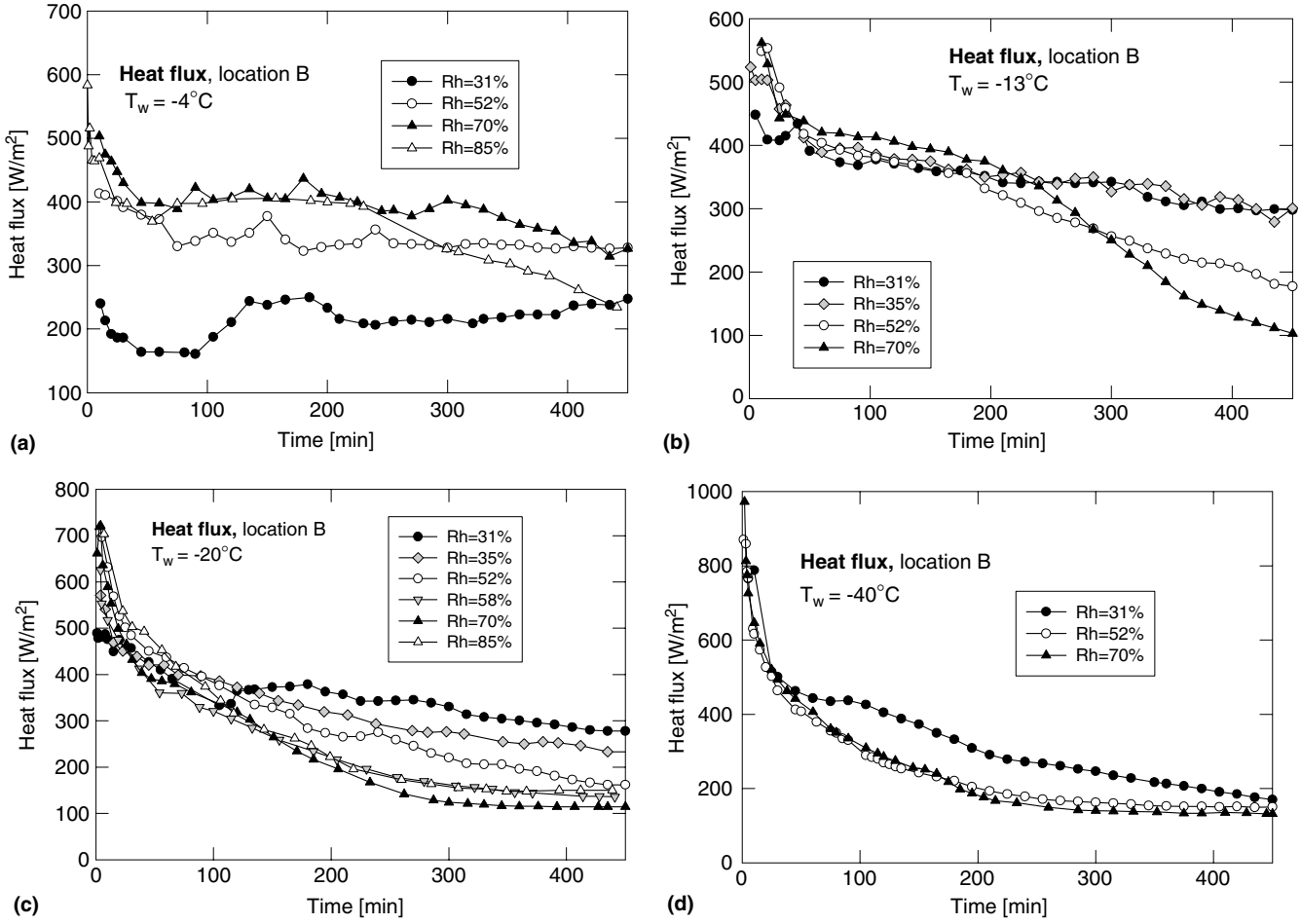

Fig. 8. Heat flux at the cold plate/frost interface versus time at different Rh. (a) $T_w = -4$ °C, (b) $T_w = -13$ °C, (c) $T_w = -20$ °C, and (d) $T_w = -40$ °C.

−20 °C, Fig. 8c and $T_w = -40$ °C, Fig. 8d), heat flux decreases even more strongly during the early stage of the transient, especially at the highest relative humidities, and reaches an asymptotic value of about 120 W/m^2 for $T_w = -20$ °C and 130 W/m^2 for $T_w = -40$ °C.

3.5. Deposited mass of frost

The deposited mass (per unit area of the cold plate) during frost growth is presented in Fig. 9. As previously mentioned, the mass was scraped off the plate and weighed; data at intermediate time values were thus obtained by performing additional runs of different duration.

As found in previous experiments for the larger (20 mm) channel [21–23], when the convection process in the channel turned out not to be significantly altered by the frost growth, the mass of frost increases almost linearly with time and almost independent of cold plate temperature. This means that the difference in vapour concentrations between the air and the frost layer (the driving force of mass transfer) does not vary considerably with time. This trend is noticeable for tests conducted at the lowest humidity (Fig. 9a) and at the intermediate humidity (Fig. 9b) with relatively high cold plate temperature. When convection is reduced (owing to the flow passage contraction), the slope of the mass rate variation with time tends to decrease; this is particularly evident at the highest humidity (Fig. 9c) and lowest cold plate temperatures.

3.6. Data reduction

Results were recast in order to identify significant parameters affecting frost thickness, mass and density with the aim to develop correlations able to predict the frost growth under given ambient (temperature and relative humidity) and cold plate (temperature) conditions.

A parameter affecting the frost layer thickness has been obtained on a theoretical basis by Schneider [24] and used by Cremers and Mehra [20] to correlate the thickness for free-convective frost formation on vertical cylinders in the 65–94% relative humidity range. This parameter, termed FGP (frost growth parameter), is given by the product of the time measured from inception of growth and the temperature difference across the frost layer:

$$\mathrm{FGP} = \tau \cdot (T_{fs} - T_w) \tag{1}$$

The frost growth parameter arises from the assumption that the heat delivered by condensation into the solid phase

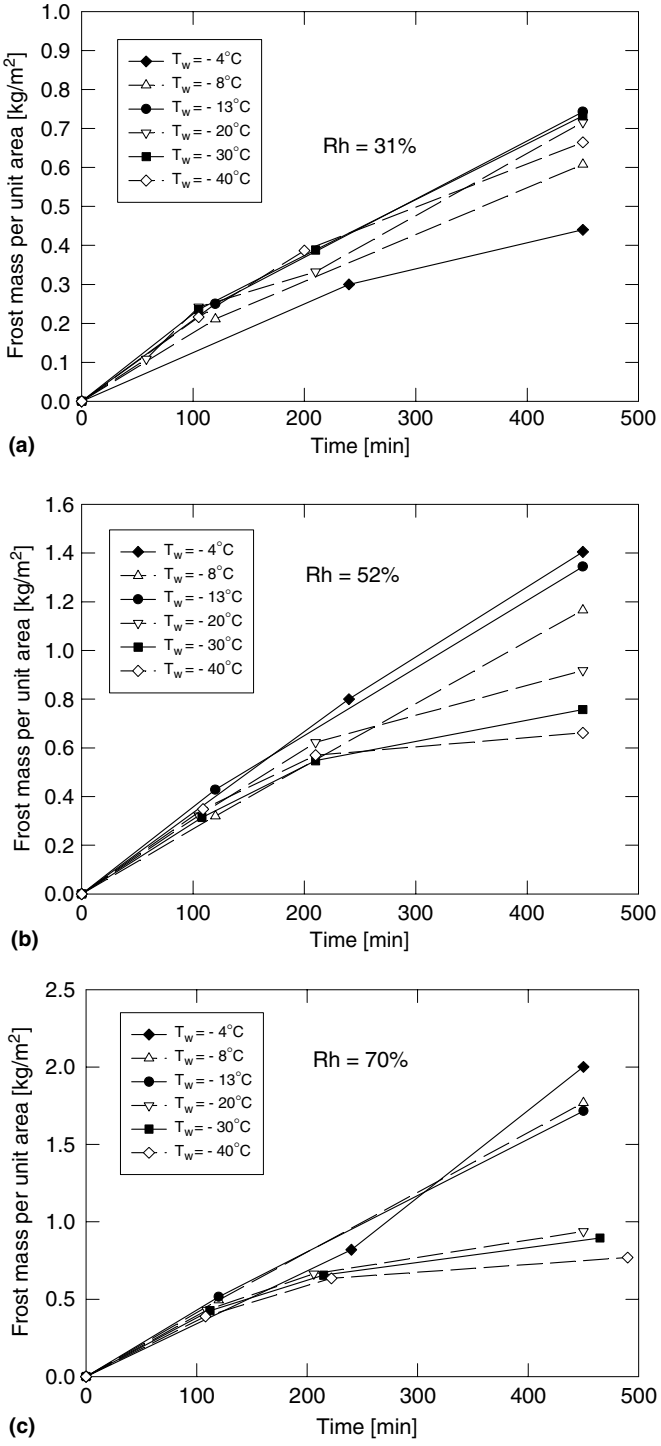

Fig. 9. Amount of deposited mass of frost with time at different T_w. (a) Rh = 31%, (b) 52%, and (c) 70%.

is transferred to the cold plate by conduction across the frost layer; in [20,24] it was found to correlate the frost layer thickness according to a power law with an exponent in the 0.4–0.5 range.

Fig. 10 shows the mean frost thickness δ (in mm) obtained from the present experiment as a function of FGP (in min K). A least-squares analysis of data, excluding

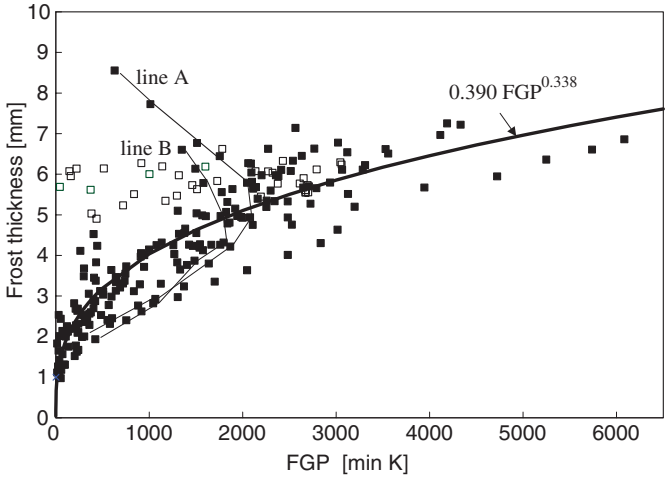

Fig. 10. Frost growth correlation: mean thickness versus FGP (frost growth parameter). Filled symbols: uniform frost growth; open symbols: irregular frost growth with flow blockage. Lines A and B: typical runs with non-biunivocal correspondence of the thickness–FGP relation.

the values recorded after the flow blockage (open symbols), resulted in the following relationship

$$\delta = 0.390\mathrm{FGP}^{0.338} \tag{2}$$

characterised by a coefficient of correlation r equal to 0.828 and a standard error of estimate S equal to 0.963 mm. However, FGP seems to be inadequate to correlate the frost thickness for the following reasons: (i) no indication concerning the occurrence of flow blockage is inferred by the value of FGP, (ii) in some experimental runs (line A, Rh = 70% and $T_w = -13$ °C and line B, Rh = 70% and $T_w = -8$ °C in Fig. 10) in which the frost grows uniformly but convection is markedly reduced due to the free-flow area contraction, the temperature difference across the layer, beyond a critical time, decreases faster than the increase in time, leading to a non-biunivocal correspondence between FGP and frost thickness. It can be concluded that relationships based on FGP may fail to predict the frost thickness in channels owing to the alterations induced by the free-flow area contraction in the convective air flow. Moreover, FGP use could be impractical in real situations since the frost surface temperature, on which FGP depends, is typically unknown. A different approach has been followed to correlate the frost layer thickness to input data as will be described later.

The mass flux of sublimating water vapour depends on the difference between the vapour concentration of the air flow and the vapour concentration of the air in contact with the frost surface. Therefore, a parameter, termed MDP (mass deposition parameter), affecting the deposited mass of frost can be defined as follows:

$$\mathrm{MDP} = \tau \cdot [\omega(T_{\mathrm{amb}}) - \omega(T_{\mathrm{fs}})] \tag{3}$$

where τ is the time expressed in min, $\omega(T_{\mathrm{amb}})$ is the air humidity ratio, in $\mathrm{kg_v/kg}$, measured at ambient (inlet) temperature T_{amb} and relative humidity Rh, while $\omega(T_{\mathrm{fs}})$ is the

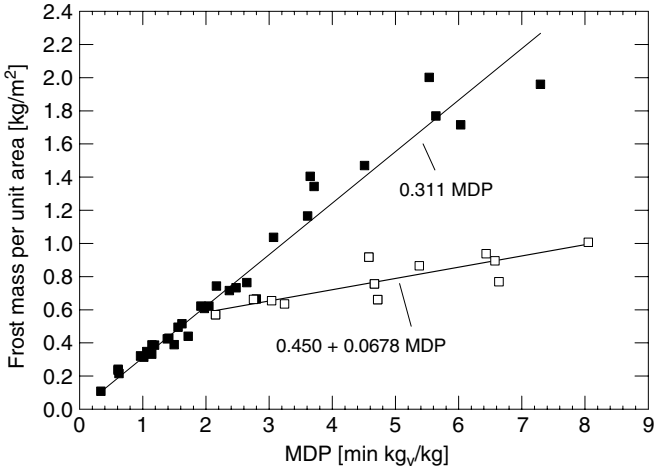

Fig. 11. Deposited frost mass correlation: mass versus MDP (mass deposition parameter). Filled symbols: uniform frost growth; open symbols: irregular frost growth with flow blockage.

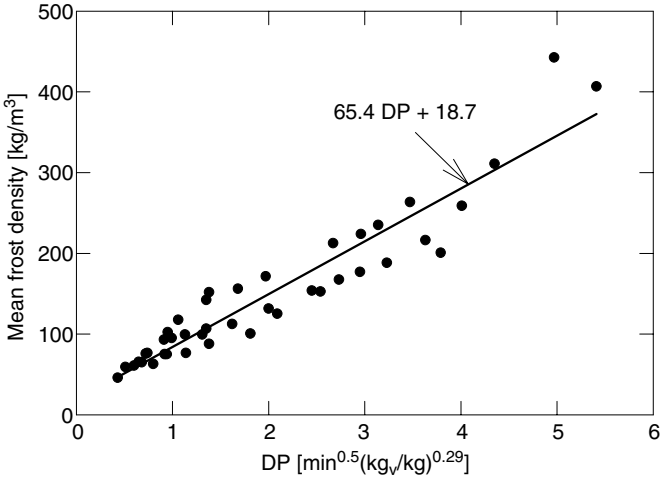

Fig. 12. Mean frost density correlation: density versus DP (densification parameter); all experimental runs.

air humidity ratio, in kg_v/kg, at frost air/interface (temperature T_{fs} and relative humidity 100%.)

Frost mass data (per unit area) m'' (in kg/m^2) have been plotted in Fig. 11 against MDP. When MDP is lower than 2 min kg_v/kg, mass data are fitted by the following relationship:

$$m'' = 0.311 \cdot \mathrm{MDP} \tag{4}$$

with coefficient of correlation $r = 0.979$ and standard error of estimate $S = 0.111\ kg/m^2$.

For highest values of MDP, Eq. (4) still holds for data obtained after a uniform growth of the frost (closed symbols) while the occurrence of the flow blockage effect at the plate leading edge leads to a slower increase in the deposited mass (open symbols), according to the following expression:

$$m'' = 0.0678 \cdot \mathrm{MDP} + 0.450 \tag{5}$$

with coefficient of correlation $r = 0.852$ and standard error of estimate $S = 0.079\ kg/m^2$.

The same correlation applies when the humidity ratio $\omega(T_{fs})$ is estimated at the temperature $T_{fs} = (273 + T_w)/2$, that represents a rough evaluation of the frost surface temperature. This is due to the fact that $\omega(T_{amb})$ is typically much larger than $\omega(T_{fs})$ so an error in the latter term does not significantly affect MDP. Eqs. (4) and (5) can thus be used to predict the deposited mass of frost as a function of environmental conditions (T_{amb}, Rh and T_w).

The mean density ρ of the frost layer can be directly obtained from experiments as the ratio between the frost mass (per unit area) m'' (in kg/m^2) and the mean frost thickness δ (in mm):

$$\rho = m''/(\delta \times 10^{-3}) \tag{6}$$

A systematic analysis of all density data (including those recorded after the blockage of the channel) led to the definition of a parameter (termed DP, densification parameter) given by

$$\mathrm{DP} = \tau^a \cdot (T_w/273)^b \cdot [\omega(T_{amb}) - \omega(T_{fs})]^c \tag{7}$$

where τ is expressed in min, T_w in K, and ω is the air humidity ratio, measured in kg_v/kg, at ambient conditions (T_{amb}, Rh) and at frost surface conditions (T_{fs}, Rh = 100%). The optimised values of the exponents are: $a = 0.5$, $b = 10.22$, $c = 0.29$. According to the above definition of DP, the mean density of frost, plotted in Fig. 12, is given by

$$\rho = 65.4\mathrm{DP} + 18.7 \tag{8}$$

where ρ is in kg/m^3. The coefficient of correlation r and the standard error of estimate S are 0.949 and 28.9 kg/m^3, respectively.

As done for MDP, it is reasonable to evaluate DP using for T_{fs} the mean value between the cold plate temperature and the freezing temperature ($T_{fs} = (273 + T_w)/2$); again, an error in $\omega(T_{fs})$ has a little impact on $[\omega(T_{amb}) - \omega(T_{fs})]^{0.29}$, consequently Eq. (8) can be used to evaluate the frost density as a function of ambient temperature, relative humidity and cold plate temperature.

The dependence of frost mass and density on MDP and DP respectively, has led the authors to introduce a novel parameter (termed FTP, frost thickness parameter), to correlate the frost thickness, given by the ratio between MDP and DP:

$$\mathrm{FTP} = \mathrm{MDP}/\mathrm{DP} = \tau^{0.5} \cdot (273/T_w)^{10.22} \cdot [\omega(T_{amb}) - \omega(T_{fs})]^{0.71} \tag{9}$$

The measured mean frost thickness versus FTP is shown in Fig. 13. The frost surface temperature employed in Eq. (9) is the mean between T_w and 273 (not the measured value of T_{fs}) so as to relate FTP to input data T_{amb}, Rh and T_w. As emerges from inspection of the figure, the frost thickness appears to be linearly correlated to FTP when FTP is lower than a critical value, probably controlled by the geometry of the channel, here approximately equal to 1.5. The resulting empirical relation is

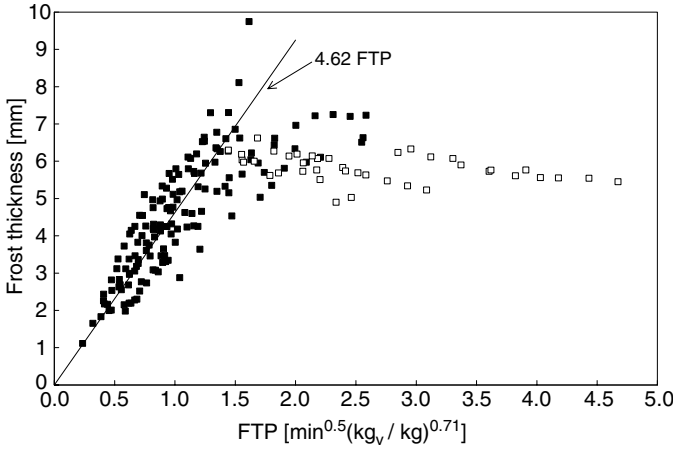

Fig. 13. Mean frost thickness correlation: thickness versus FTP (frost thickness parameter). The frost surface temperature T_{fs} used in FTP is here approximated as $(273 + T_w)/2$. Filled symbols: uniform frost growth; open symbols: irregular frost growth with flow blockage.

$$\delta = 4.62\mathrm{FTP} \tag{10}$$

where δ is in mm. The coefficient of correlation r and the standard error of estimate S are 0.841 and 0.76 mm, respectively. Since for values of FTP exceeding 1.5, the frost growth is not regular as explained in Paragraph 3.1, the prediction of δ through FTP is reliable in the FTP range from 0 to 1.5.

4. Conclusions

Frost growth process on a vertical cooling surface in free convection has been experimentally investigated. The cooling surface was placed in a narrow (10 mm wide) vertical channel open at the top and bottom in order to permit the natural circulation of ambient air. The cooling surface temperature and the air relative humidity were varied in the −40 to −4 °C and 31–85% range, respectively, while the ambient air temperature was held fixed at 27 °C (±1 °C).

Relative to studies on free convection frost growth over isolated surfaces, the presence of the confinement induced by the narrow channel was found to remarkably alter the process, especially at the lowest cold plate temperatures here explored, combined with relatively high levels of the air relative humidity. Two typical frost outlines were identified: (i) a uniform frost layer growing over the cooling surface, which progressively reduces the down-moving buoyant air flow as the free flow passage is reduced and (ii) an abrupt growth at the leading edge of the cooling surface that, in a relatively short transient, causes an obstruction to the buoyant flow with consequent interruption of frost growth and sudden reduction in heat flux from air to the cooling plate. The occurrence of a given frost outline has been related to the input conditions, i.e. the values of ambient air relative humidity and cold plate temperature.

Experiments have been recast in order to envisage compact parameters useful for the prediction of frost growth inside narrow channels. Even though the physics of the phenomenon indicates the frost surface temperature (typically unknown in practical situations) as one of the significant variables affecting the frost growth, correlations giving the time evolution of deposited mass, mean density and mean thickness of frost as a function of the input data (ambient air temperature and relative humidity, and cold plate temperature) have been provided. In particular, a densification parameter (DP) was introduced to correlate the mean frost density under any frost growth condition (with and without flow blockage), while the mass deposition parameter (MDP) and the frost thickness parameter (FTP) allow the estimation of the frost deposited mass and mean thickness, respectively, in the case of uniform frost growth (i.e. within limiting values of MDP and FTP). A convenient frost surface temperature (given by the average between the cold plate and the freezing temperature) can be used in the empirical relations to overcome the difficulty of knowing this variable a priori.

References

[1] Y. Hayashi, A. Aoki, S. Adachi, K. Hori, Study of frost properties correlating with frost formation types, ASME Journal of Heat Transfer 99 (1977) 239–245.
[2] I. Tokura, H. Saito, K. Kishinami, Prediction of growth rate and density of frost layer developing under forced convection, Waerme und Stoffuebertragung 22 (1988) 285–290.
[3] D.L. O'Neal, D.R. Tree, Measurement of frost growth and density in a parallel plate geometry, ASHRAE Transactions 90 (Part 2) (1984) 278–290.
[4] R. Ostin, S. Andersson, Frost growth parameters in a forced air stream, International Journal of Heat Mass Transfer 34 (1991) 1009–1017.
[5] Y.B. Lee, S.T. Ro, Frost formation on a vertical plate in simultaneously developing flow, Experimental Thermal and Fluid Science 26 (2002) 939–945.
[6] A.Z. Sahin, An experimental study on the initiation and growth of frost formation on a horizontal plate, Experimental Heat Transfer 7 (1994) 101–119.
[7] I. Tokura, H. Saito, K. Kishinami, Study on properties and growth rate of frost layers on cold surfaces, ASME Journal of Heat Transfer 105 (1983) 895–901.
[8] Y.X. Tao, R.W. Besant, Y. Mao, Characteristics of frost growth on a flat plate during the early growth period, ASHRAE Transactions 99 (1993) 746–753.
[9] B.W. Jones, J.D. Parker, Frost formation with varying environmental parameters, ASME Journal of Heat Transfer 97 (1975) 255–259.
[10] M.M. Padki, S.A. Sherif, R.M. Nelson, A simple method for modeling the frost formation phenomenon in different geometries, ASHRAE Transactions 95 (1989) 1127–1137.
[11] Y.X. Tao, R.W. Besant, K.S. Rezkallah, A mathematical model for predicting the densification and growth of frost on a flat plate, International Journal of Heat and Mass Transfer 36 (1993) 353–363.
[12] R. LeGall, M. Grillot, C. Jallut, Modelling of frost growth and densification, International Journal of Heat and Mass Transfer 40 (1997) 3177–3187.
[13] K.S. Lee, W.S. Kim, T.H. Lee, A one-dimensional model for frost formation on a cold flat surface, International Journal of Heat and Mass Transfer 40 (1997) 4359–4365.
[14] R. Yun, Y. Kim, M. Min, Modeling of frost growth and frost properties with airflow over a flat plate, International Journal of Refrigeration 25 (2002) 362–371.
[15] B. Na, R.L. Webb, New model for frost growth rate, International Journal of Heat and Mass Transfer 47 (2004) 925–936.

[16] D.L. O'Neal, D.R. Tree, A review of frost formation in simple geometries, ASHRAE Transactions 91 (1985) 267–281.
[17] S. Mishra, A. Gidwani, M.M. Ohadi, S.V. Dessiatoun, An overview of basic models of frost formation phenomenon and recent progress on the use of an electric field in suppressing or promoting frost, in: Proceedings of the AIChE Symp. Series Heat Transfer, Baltimore, USA, 1997, vol. 93, pp. 197–210.
[18] L.A. Kennedy, J. Goodman, Free convection heat and mass transfer under conditions of frost deposition, International Journal of Heat and Mass Transfer 17 (1974) 477–484.
[19] O. Tajima, E. Naito, K. Nakashima, H. Yamamoto, Frost formation on air coolers. Part 3: natural convection for a cooled vertical plate, Heat Transfer Japanese Research 3 (1974) 55–66.
[20] C.J. Cremers, V.K. Mehra, Frost formation on vertical cylinders in free convection, ASME Journal of Heat Transfer 104 (1982) 3–7.
[21] G. Tanda, M. Fossa, An experimental study of the frost formation on a cold surface in free convective flow, in: Proceedings of the 5th World Conf. on Experimental Heat Transfer, Fluid Mechanics and Thermodynamics, Thessaloniki, Greece, 2001, vol. 1, pp. 693–697.
[22] M. Fossa, G. Tanda, Free convection frost formation on a cold plate in a vertical channel, in: Proceedings of 1st Int. Conf. on Heat Transfer, Fluid Dynamics and Thermodynamics (HEFAT), Kruger Nat. Park, South Africa, 2002, vol. 1, Part 1, pp. 696–701.
[23] M. Fossa, G. Tanda, Study of the free convection frost formation on a vertical plate, Experimental Thermal and Fluid Science 26 (2002) 661–668.
[24] H.W. Schneider, Equation of the growth rate of frost forming on cooled surfaces, International Journal of Heat and Mass Transfer 21 (1978) 1019–1024.